

Charge asymmetry of heavy quarks at hadron colliders

J. H. Kühn

Institut für Theoretische Teilchenphysik, Universität Karlsruhe, D-76128 Karlsruhe, Germany

G. Rodrigo

INFN-Sezione di Firenze, Largo E. Fermi 2, I-50125 Firenze, Italy

(Received 21 July 1998; published 8 February 1999)

A sizable difference in the differential production cross section of top quarks and top antiquarks, respectively, is predicted for hadronically produced heavy quarks. It is of order α_s and arises from the interference between charge odd and even amplitudes, respectively. For the Fermilab Tevatron it amounts up to 15% for the differential distribution in suitable chosen kinematical regions. The resulting integrated forward-backward asymmetry of 4–5% could be measured in the next round of experiments. At the CERN LHC the asymmetry can be studied by selecting appropriately chosen kinematical regions. Furthermore, a slight preference at LHC for a centrally produced top antiquark is predicted, with top quarks more abundant at large positive and negative rapidities. [S0556-2821(99)04805-5]

PACS number(s): 14.65.Ha, 12.38.Bx, 12.38.Qk, 13.87.Ce

I. INTRODUCTION

Heavy flavor production at hadron colliders is one of the most active fields of current theoretical and experimental studies. Large event rates, combined with improved experimental techniques, allow for detailed investigations of the properties of heavy quarks and their production mechanism at the same time. While charm quark production with a quark mass around 1.5 GeV is barely accessible to perturbative QCD calculations, bottom and *a fortiori* top quark production should be well described by this approach.

Theoretical and experimental results [1,2] for the cross section of hadronic top quark production are well consistent with this expectation. Obviously, in view of the large QCD coupling, the inclusion of higher order QCD corrections in these calculations is mandatory for a successful comparison. Recent studies have, to a large extent, concentrated on the predictions of the total cross section and a few selected one-particle inclusive distributions. In this paper a different issue of heavy flavor production is investigated, namely, the charge asymmetry, which is sensitive toward a specific subclass of virtual and real radiative corrections.

Evaluated in the Born approximation the lowest order processes relevant for heavy flavor production,

$$q + \bar{q} \rightarrow Q + \bar{Q}, \quad (1)$$

$$g + g \rightarrow Q + \bar{Q}, \quad (2)$$

do not discriminate between the final quark and antiquark, thus predicting identical differential distributions also for the hadronic production process. However, radiative corrections involving either virtual or real gluon emission lead to a sizable difference between the differential quark and antiquark production processes and hence to a charge asymmetry which could be well accessible experimentally.

This asymmetry has its origin in two different reactions: radiative corrections to quark-antiquark fusion (Fig. 1) and heavy flavor production involving interference terms of different amplitudes contributing to gluon-quark scattering (Fig. 2),

$$g + q \rightarrow Q + \bar{Q} + q, \quad (3)$$

a reaction intrinsically of order α_s^3 . Gluon fusion remains of course charge symmetric. In both reactions (1) and (3) the asymmetry can be traced to the interference between amplitudes which are relatively odd under the exchange of Q and \bar{Q} . In fact, as shown below in detail, the asymmetry can be understood in analogy to the corresponding one in QED reactions and is proportional to the color factor d_{abc}^2 . In contrast, the non-Abelian contributions, in particular those involving the triple-gluon coupling, lead to symmetric pieces in the differential cross section. Event generators which do

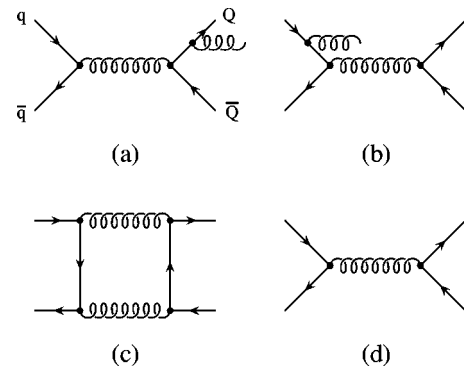


FIG. 1. Origin of the QCD charge asymmetry in hadroproduction of heavy quarks: interference of final-state (a) with initial-state (b) gluon bremsstrahlung plus interference of the box (c) with the Born diagram (d). Only representative diagrams are shown.

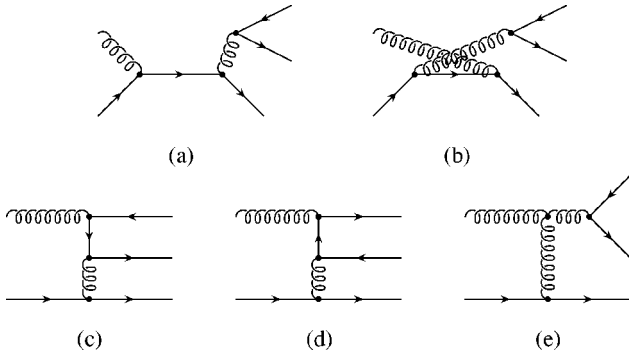


FIG. 2. Origin of the QCD charge asymmetry in hadroproduction of heavy quarks through flavor excitation.

not include the full next-to-leading matrix elements [3,4] cannot predict the asymmetry.

Let us briefly discuss a few important aspects of this calculation. The box amplitude for $q\bar{q} \rightarrow Q\bar{Q}$ is ultraviolet finite and the asymmetric contribution to the cross section of order α_s^3 is therefore not affected by renormalization, an obvious consequence of the symmetry of the lowest order reaction. The same line of reasoning explains the absence of initial-state collinear singularities in the limit $m_q \rightarrow 0$ which would have to be absorbed into the (symmetric) lowest order cross section. Infrared singularities require a more careful treatment. They are absent in the asymmetric piece of the process in Eq. (3). However, real and virtual radiation (Fig. 1), if considered separately, exhibit infrared divergences, which compensate in the sum, corresponding to the inclusive production cross section.

The charge asymmetry in the partonic reactions (1) and (3) implies, for example, a forward-backward asymmetry of heavy flavor production in proton-antiproton collisions. In particular, it leads to a sizable forward-backward asymmetry for top quark production which is dominated by reaction (1), and can, furthermore, be scrutinized by studying $t\bar{t}$ production at fixed longitudinal momenta and at various partonic energies \hat{s} . However, the charge asymmetry can also be observed in proton-proton collisions at high energies. In this case one has to reconstruct the $t\bar{t}$ rest frame and select kinematic regions, which are dominated by $q\bar{q}$ annihilation or flavor excitation $gq \rightarrow t\bar{t}X$. Alternatively, one may also study the difference in the one-particle inclusive rapidity distribution of a top quark versus a top antiquark, which again integrates to zero.

The analysis of these effects allows to improve our understanding of the QCD production mechanism. At the same time it is important for the analysis of single-top-quark production through Wb fusion. This reaction is charge asymmetric as a consequence of weak interactions. Although the final states in single-top-quark production and hadronic $t\bar{t}$ production are different and should in principle be distinguishable, it is nevertheless mandatory to control the charge asymmetry from both sources.

The presence of charge-asymmetric contributions in the flavor excitation reaction has also been noticed in [5–7] for b quark production, however without any quantitative state-

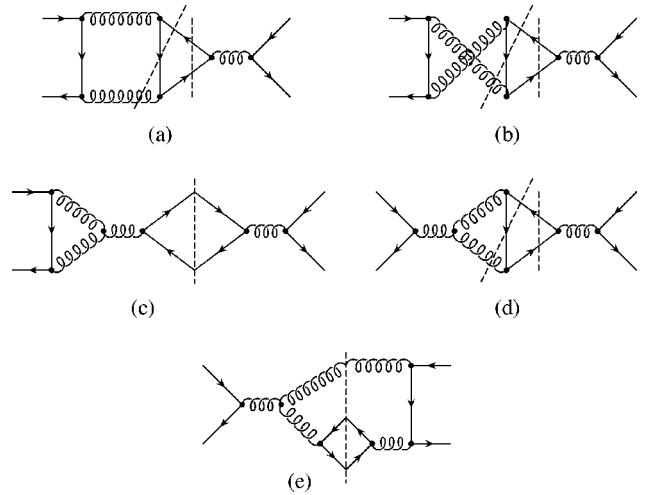


FIG. 3. Cut diagrams.

ment. The charge asymmetry was also investigated in [8]. In this work only real gluon emission was considered. To arrive at a finite result, a gluon energy infrared cut E_{cut} had to be introduced which leads to arbitrary large results with a pronounced dependence on E_{cut} and a different sign of the asymmetry compared to our inclusive calculation.

The outline of this paper is as follows. The technical aspects of the calculations will be presented in Sec. II. The asymmetric pieces of real and virtual corrections will be given, together with the numerical evaluation, the compensation of infrared singularities from real and virtual radiation, and the results at the partonic level. The implications for hadronic collisions, proton-proton as well as proton-antiproton, will be studied in Sec. III. A brief summary and our conclusions will be given in Sec. IV.

The main thrust of this paper is toward the study of top quarks. Nevertheless, all the results are in principle applicable to bottom and charm quarks. In practice, of course kinematical regions have to be selected, which are dominated by $q\bar{q}$ annihilation or flavor excitation. For b quarks, furthermore, the dilution effects of mixing must be included. We will comment on these points in more detail below.

II. AMPLITUDES AND PARTONIC CROSS SECTION

As we shall see below, the dominant contribution to the charge asymmetry originates from $q\bar{q}$ annihilation, namely, from the asymmetric piece in the interference between the Born amplitude for $q\bar{q} \rightarrow Q\bar{Q}$ (Fig. 1d) and the one loop corrections to this reaction (Fig. 1c), which must be combined with the interference term between initial state and final state radiation (Figs. 1a,1b). The corresponding contribution to the rate is conveniently expressed by the absorptive contributions (cuts) of the diagrams depicted in Figs. 3a–3e.

However, only Fig. 3a plus the crossed Fig. 3b are relevant for the charge asymmetric piece. Figures 3c, 3d, and 3e, on the other hand, lead to a symmetric contribution only. This can be seen as follows: the color factors corresponding to Figs. 3a and 3b (after averaging over initial and summing over final states), respectively, are given by

$$\begin{aligned}
C_{3a} &= \frac{1}{N_C^2} \text{Tr} \left(\frac{\lambda^a}{2} \frac{\lambda^b}{2} \frac{\lambda^c}{2} \right) \text{Tr} \left(\frac{\lambda^a}{2} \frac{\lambda^c}{2} \frac{\lambda^b}{2} \right) \\
&= \frac{1}{16N_C^2} (f_{abc}^2 + d_{abc}^2), \\
C_{3b} &= \frac{1}{N_C^2} \text{Tr} \left(\frac{\lambda^a}{2} \frac{\lambda^b}{2} \frac{\lambda^c}{2} \right) \text{Tr} \left(\frac{\lambda^b}{2} \frac{\lambda^c}{2} \frac{\lambda^a}{2} \right) \\
&= \frac{1}{16N_C^2} (-f_{abc}^2 + d_{abc}^2), \tag{4}
\end{aligned}$$

where $N_C=3$, $f_{abc}^2=24$, and $d_{abc}^2=40/3$. Without color factors the contributions to the cross section from Figs. 3a and 3b are related by

$$d\sigma_{3a}(Q, \bar{Q}) = -d\sigma_{3b}(\bar{Q}, Q), \tag{5}$$

which holds true both for two- and three-particle cuts. The asymmetric piece thus originates from the d_{abc}^2 term, and its form is thus equivalent to the corresponding QED reaction with the replacement of the quark charges and QED coupling by the color factor

$$\alpha_{QED}^3 Q_q^3 Q_{\bar{Q}}^3 \rightarrow \frac{1}{N_C^2} \frac{1}{16} d_{abc}^2 \alpha_s^3. \tag{6}$$

The production cross section, on the other hand, is obtained from the corresponding QED process through the replacement

$$\alpha_{QED}^2 Q_q^2 Q_{\bar{Q}}^2 \rightarrow \frac{1}{N_C^2} N_C T_F C_F \alpha_s^2, \tag{7}$$

with $T_F=1/2$, $C_F=4/3$. The QCD asymmetry is thus obtained from the QED results by the replacement

$$\alpha_{QED} Q_q Q_{\bar{Q}} \rightarrow \frac{d_{abc}^2}{16N_C T_F C_F} \alpha_s = \frac{5}{12} \alpha_s. \tag{8}$$

Let us note in passing that the cuts through diagrams involving the triple gluon coupling (Figs. 3c,3d,3e) lead to charge symmetric terms. For Figs. 3c and 3e this can be seen as follows: its contribution involves the factor $\text{Tr} \{ \gamma^\alpha (\not{Q} + M) \gamma^\beta (\not{\bar{Q}} - M) \}$ which is evidently symmetric under the exchange of Q and \bar{Q} . The remainder of the diagram depends on $Q + \bar{Q}$ only, which leads to the charge symmetry of the whole amplitude. The same line of reasoning applies to Fig. 3d, as far as the exchange of the initial quarks is concerned. Charge conjugation invariance then implies that also Fig. 3d is symmetric under the exchange between Q and \bar{Q} . These terms have to be combined with the charge-symmetric $C_F C_A$ terms from Figs. 3a and 3b to yield a gauge-invariant combination.

Although the relevant ingredients for the charge-asymmetric piece are already listed in the original QED pub-

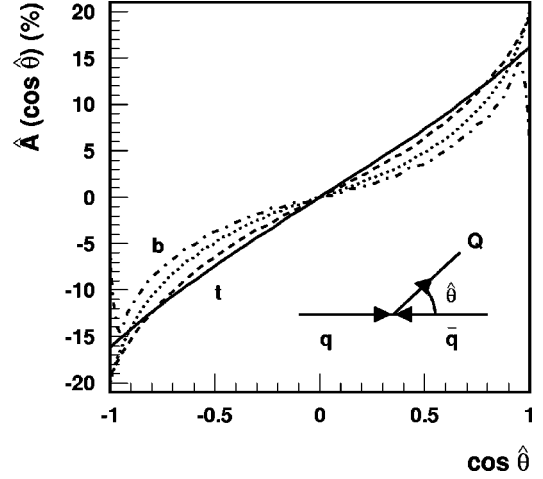


FIG. 4. Differential charge asymmetry in top quark pair production for fixed partonic center-of-mass energies $\sqrt{\hat{s}}=400$ GeV (solid line), 600 GeV (dashed line), and 1 TeV (dotted line). We also plot the differential asymmetry for b quarks with $\sqrt{\hat{s}}=400$ GeV (dash-dotted line).

lications [9,10] (and the later works on hadronic heavy flavor production in [5–8]), the compact formulas shall be listed in the Appendix for completeness and convenience of the reader. In a first step virtual and soft radiation are combined, with a cut on the gluon energy, E_{cut}^g [see the Appendix, Eq. (A5)]. The logarithmic divergence of this result for small E_{cut}^g is cancelled by the corresponding divergence for real radiation. A particularly compact formula for the asymmetric piece of the hard radiation is given in Eq. (A3). To obtain finally the asymmetric piece of the inclusive cross section for

$$q + \bar{q} \rightarrow Q + X, \tag{9}$$

the integral over the real gluon spectrum is performed numerically.

The differential charge asymmetry at the partonic level can then be defined through

$$\hat{A}(\cos \hat{\theta}) = \frac{N_t(\cos \hat{\theta}) - N_{\bar{t}}(\cos \hat{\theta})}{N_t(\cos \hat{\theta}) + N_{\bar{t}}(\cos \hat{\theta})}, \tag{10}$$

where $\hat{\theta}$ denotes the top quark production angle in the $q\bar{q}$ rest frame and $N(\cos \hat{\theta}) = d\sigma/d\Omega(\cos \hat{\theta})$. Since $N_{\bar{t}}(\cos \hat{\theta}) = N_t(-\cos \hat{\theta})$ as a consequence of charge conjugation symmetry, $\hat{A}(\cos \hat{\theta})$ can also be interpreted as a forward-backward asymmetry of top quarks. In this case the denominator is of course given by the Born cross section for the reaction $q\bar{q} \rightarrow Q\bar{Q}$ [see Eq. (A14)]. In Fig. 4, $\hat{A}(\cos \hat{\theta})$ is displayed for $\sqrt{\hat{s}}=400$ GeV, 600 GeV, and 1 TeV for $m_t=175$ GeV. For completeness we also display the result for $b\bar{b}$ production at $\sqrt{\hat{s}}=400$ GeV with $m_b=4.6$ GeV. The strong coupling constant is evaluated at the scale $\mu = \sqrt{\hat{s}}/2$ from $\alpha_s(m_Z) = 0.118$.

The integrated charge asymmetry

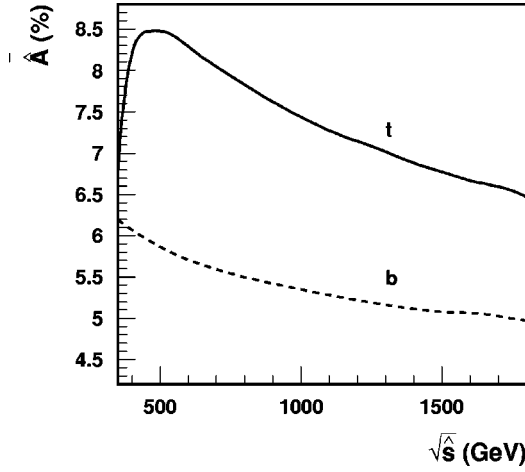


FIG. 5. Integrated charge asymmetry as a function of the partonic center-of-mass energy for top and bottom quark pair production.

$$\bar{A} = \frac{N_t(\cos \hat{\theta} \geq 0) - N_{\bar{t}}(\cos \hat{\theta} \geq 0)}{N_t(\cos \hat{\theta} \geq 0) + N_{\bar{t}}(\cos \hat{\theta} \geq 0)} \quad (11)$$

is shown in Fig. 5 as a function of $\sqrt{\hat{s}}$. With a typical value of around 6–8.5% it should be well accessible in the next run of the Fermilab Tevatron.

As mentioned already in the Introduction, the asymmetric piece does not exhibit a divergence, even in the limit of vanishing initial quark mass; in other words, no collinear singularities arise. The virtual plus soft radiation on the one hand and the real hard radiation on the other contribute with opposite signs, with the former always larger than the latter which explains the difference in sign between our result and [8].

Before moving to the application of these results by folding with the parton distribution functions let us first discuss the charge asymmetry in the quark-gluon-induced reaction in Eq. (3). The cross section for this reaction is obtained from the amplitudes depicted in Fig. 2. In fact its antisymmetric piece can be obtained by crossing directly from the reaction $q\bar{q} \rightarrow Q\bar{Q}g$ and is given by Eq. (A13). Again only the QED like piece contributes to the asymmetry, in contrast to those amplitudes induced by the triple-gluon coupling. The inclusive cross section for quark production in quark-gluon collisions exhibits a collinear divergence; the charge asymmetric piece is finite. The difference between Q and \bar{Q} production (for fixed initial q and gluon directions) should not be confused with an asymmetry in the angular distribution of Q (or \bar{Q}), which is a trivial consequence of the asymmetric initial state configuration.

The charge-asymmetric pieces as a function of the scattering angle,

$$\frac{1}{2} \left(\frac{d\sigma(q\bar{q} \rightarrow QX)}{d \cos \hat{\theta}} - \frac{d\sigma(q\bar{q} \rightarrow \bar{Q}X)}{d \cos \hat{\theta}} \right) \equiv \frac{d\sigma_A^{q\bar{q}}}{d \cos \hat{\theta}}, \quad (12)$$

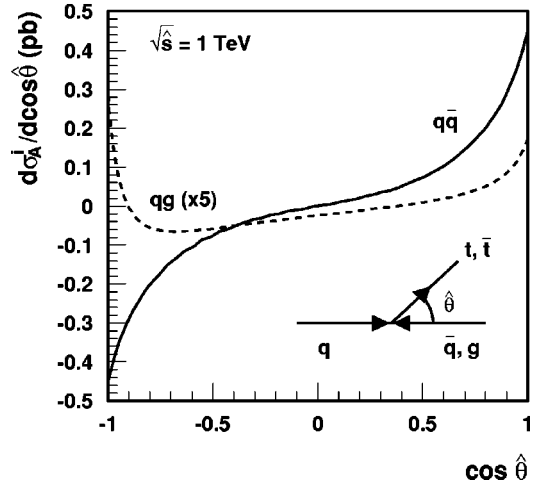
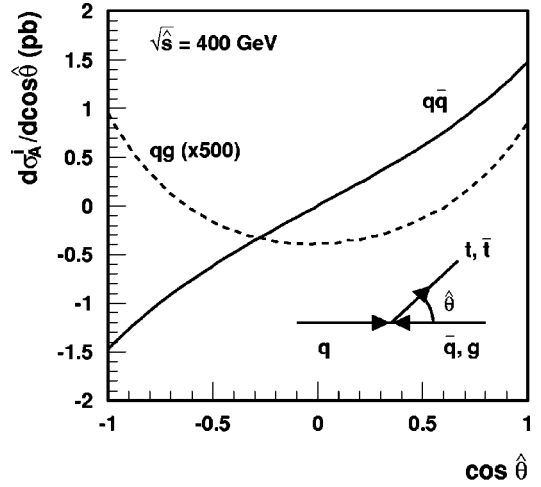


FIG. 6. Asymmetric parts of the differential top quark pair production cross section from $q\bar{q}$ - and qg -initiated processes for fixed partonic center-of-mass energies $\sqrt{\hat{s}} = 400$ GeV and 1 TeV.

$$\frac{1}{2} \left(\frac{d\sigma(qg \rightarrow QX)}{d \cos \hat{\theta}} - \frac{d\sigma(qg \rightarrow \bar{Q}X)}{d \cos \hat{\theta}} \right) \equiv \frac{d\sigma_A^{qg}}{d \cos \hat{\theta}}, \quad (13)$$

are shown in Fig. 6 for a variety of partonic energies $\sqrt{\hat{s}}$ with $m_t = 175$ GeV.

The asymmetric contributions integrated in the forward-backward direction,

$$\sigma_A^i = \int_0^1 \frac{d\sigma_A^i}{d \cos \hat{\theta}} d \cos \hat{\theta} - \int_{-1}^0 \frac{d\sigma_A^i}{d \cos \hat{\theta}} d \cos \hat{\theta}, \quad i = q\bar{q}, qg, \quad (14)$$

are shown in Fig. 7. Clearly, at the Tevatron energies with $\sqrt{\hat{s}} < 2$ TeV, the dominant asymmetric contribution comes from the $q\bar{q}$ -initiated processes, even more so, since the quark-gluon luminosity in the relevant kinematic region is far below the one for quark-antiquark reactions. Furthermore, the difference between Q and \bar{Q} production in quark-

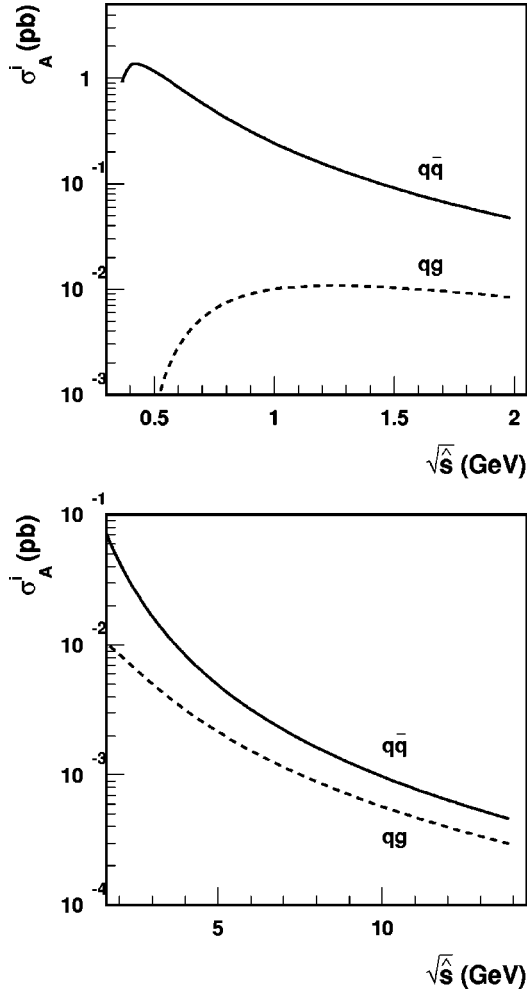


FIG. 7. Integrated charge asymmetric parts of the top quark pair production cross section from $q\bar{q}$ - and qg -initiated processes as a function of the partonic center-of-mass energy.

gluon collisions does not exhibit a marked forward-backward asymmetry, which suppresses the qg -induced asymmetry even further.

In addition to the pure QCD amplitudes also a mixed QCD-electroweak interference term will lead to an asymmetric contribution to the $q\bar{q}$ process. The QCD box diagram, Fig. 1c, can also give rise to $t\bar{t}$ in a color-singlet configuration, which in turn interferes with $t\bar{t}$ production through the photon or Z (Fig. 8a). A similar consideration applies to interference between initial- and final-state radiation. The resulting asymmetry is obtained from the QCD asymmetry through the following replacement:

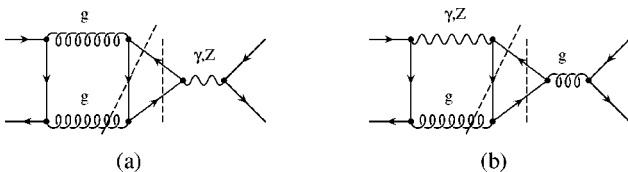


FIG. 8. Representative diagrams contributing to the QCD neutral current interference term.

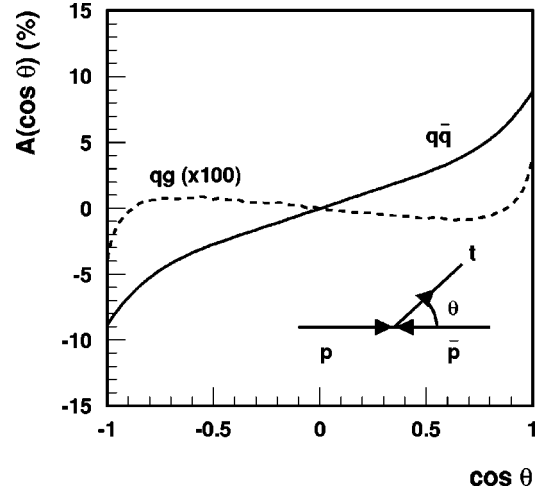


FIG. 9. Differential charge asymmetry in the proton-antiproton rest frame, $\sqrt{s}=2$ TeV, using the CTEQ-1 structure function and $\mu=m_t$. The contributions from $q\bar{q}$ - and qg - (plus $\bar{q}g$ -) initiated processes are shown separately.

$$\frac{\alpha_s}{2} \left(\frac{d_{abc}}{4} \right)^2 \rightarrow \alpha_{QED} \left(Q_t Q_q + \frac{(1 - \frac{8}{3} s_W^2)(2I_q - 4Q_q s_W^2)}{16s_W^2 c_W^2} \frac{1}{1 - \frac{m_Z^2}{\hat{s}}} \right). \quad (15)$$

Another QED-electroweak term originates from the interference between the gluon- γ box and gluon- Z box, respectively, with the QCD Born amplitude (Fig. 8b). The result for this piece¹ is also given by Eq. (15). In total this leads to an increase of the asymmetry as given by pure QCD by a factor 1.09. This change is thus smaller than uncalculated higher order corrections.

III. HADRONIC COLLISIONS

The asymmetry can in principle be studied experimentally in the partonic rest frame, as a function of \hat{s} , by measuring the invariant mass of the $t\bar{t}$ system plus an eventually radiated gluon. It is, however, also instructive to study the asymmetry in the laboratory frame by folding the angular distribution with the structure functions [11,12]. For proton-antiproton collisions it is convenient to consider the forward-backward asymmetry as function of the production angle in the center-of-mass system. The differential asymmetry for $\sqrt{s}=2$ TeV is shown in Fig. 9 which displays separately the contribution from $q\bar{q}$ - and qg - (plus $\bar{q}g$ -) initiated reactions. The denominator includes both $q\bar{q}$ - and gg -initiated processes in lowest order. The numerator is evidently dominated by quark-antiquark annihilation as anticipated in [13] as can

¹This small term had been neglected in [13].

be seen from Fig. 9. Inclusion of mixed QCD-electroweak interference term enhances the prediction by a factor of 1.09.

At this point we have to emphasize that both numerator and denominator are evaluated in leading order (LO). The next-to-leading (NLO) corrections to the $t\bar{t}$ production cross section are known to be large [14], around 30% or even more. In the absence of NLO corrections for the numerator we nevertheless stay with the LO approximation in both numerator and denominator, expecting the dominant corrections from collinear emission to cancel. However, from a more conservative point of view an uncertainty of around 30% has to be assigned to the prediction for the asymmetry.

For the total charge asymmetry at $\sqrt{s}=1.8$ TeV we predict

$$\bar{A} = \frac{N_t(\cos \theta \geq 0) - N_{\bar{t}}(\cos \theta \geq 0)}{N_t(\cos \theta \geq 0) + N_{\bar{t}}(\cos \theta \geq 0)} = 4.8 - 5.8\%, \quad (16)$$

where different choices of the structure function and different choices of the factorization and renormalization scale, $\mu = m_t/2$ and $\mu = 2m_t$, have been considered and the factor 1.09 is included. An increase in the center-of-mass energy to 2 TeV leads to a slight decrease of our prediction to 4.6–5.5%.

For illustrative purpose in Fig. 10 the $q\bar{q}$ - and qg - ($\bar{q}g$ -) induced contributions in the partonic rest frame are also displayed separately in the $x=x_1-x_2$ and \hat{s} plane for proton-antiproton collisions with $\mu = \sqrt{\hat{s}}/2$. Furthermore, as characteristic example the relative amount of gluon fusion as function of $x=x_1-x_2$ and \hat{s} is shown in the two-dimensional distribution of Fig. 11. In regions of larger $q\bar{q}$ - and correspondingly smaller gg -induced reactions a larger asymmetry is expected.

Bottom quark production at the CERN Large Hadron Collider (LHC) or Tevatron is of course dominated by gluon fusion. The forward-backward asymmetry from $q\bar{q}$ and qg ($\bar{q}g$) reactions is thus negligible, at least as far as the total cross section is concerned. However, the $b\bar{b}(g)$ final state with \hat{s} sufficiently large, say above 300 GeV, is again dominated by $q\bar{q}$ annihilation and a sizable asymmetry is predicted in this kinematical region. Selecting, for example, $\sqrt{\hat{s}} \geq 300$ GeV and $|\cos \theta| < 0.9$ one predicts ($\sqrt{s}=2$ TeV)

$$\bar{A} = 4.3 - 5.1\%, \quad (17)$$

which should be accessible by experiment. A factor 0.96, from the QCD-electroweak interference, has been also included.

Top-quark–top-antiquark production in proton-proton collisions at the LHC is, as a consequence of charge conjugation symmetry, forward-backward symmetric if the laboratory frame is chosen as the reference system. However, by selecting the invariant mass of the $t\bar{t}(+g)$ system and its longitudinal momentum appropriately, one can easily con-

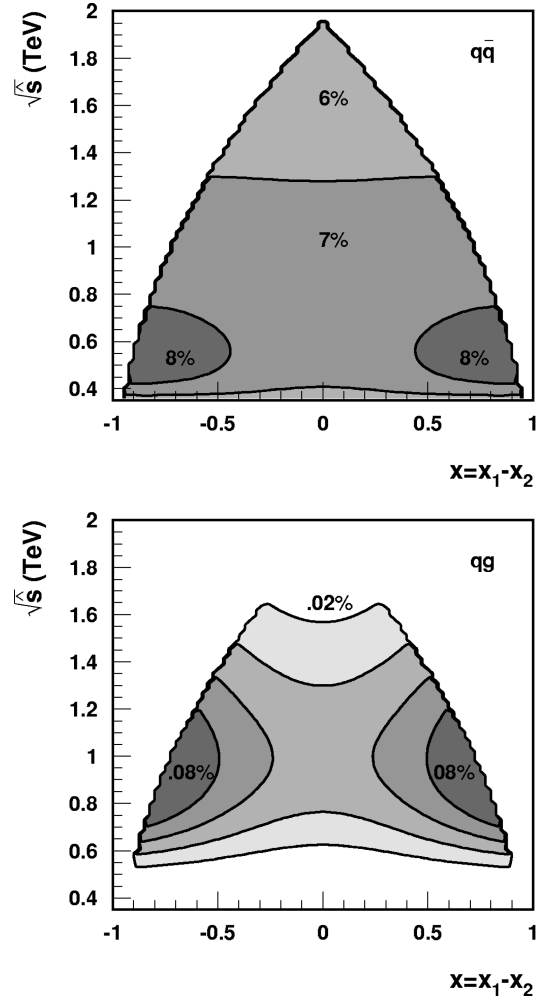


FIG. 10. Contributions from $q\bar{q}$ - and qg - ($\bar{q}g$ -) induced reactions to the charge asymmetry in proton-antiproton collisions, $\sqrt{s}=2$ TeV, as a function of $x_1-x_2=2P_3(t\bar{t}g)/\sqrt{\hat{s}}$ and \hat{s} . Partonic rest frame (CTEQ-1).

strain the parton momenta such that a preferred direction is generated for quark-antiquark reactions.

For some of the more extreme kinematical regions, namely, large x and/or large \hat{s} , a sizable difference between top quark and top antiquark production can be observed at the LHC. In Fig. 12 the contributions from $q\bar{q}$ - and qg - ($\bar{q}g$ -) induced reactions are displayed separately. The production cross section *per se*, which is decisive for the possibility of measuring the asymmetry in these regions is displayed in Fig. 14b, below. In practice, only the region with \hat{s} below 2 TeV will be observable, in particular at large x .

The asymmetry, as displayed in Fig. 12 as a function of $x=x_1-x_2$ and \hat{s} , is defined in the $t\bar{t}(g)$ rest frame. From this it may seem that the reconstruction of both t, \bar{t} and even the gluon is required for the study of the charge asymmetry in pp collisions. However, also the difference between the single-particle inclusive distribution of t and \bar{t} , respectively, may provide evidence for charge asymmetry. This can be easily understood from Fig. 13. Production of $t\bar{t}(g)$ with

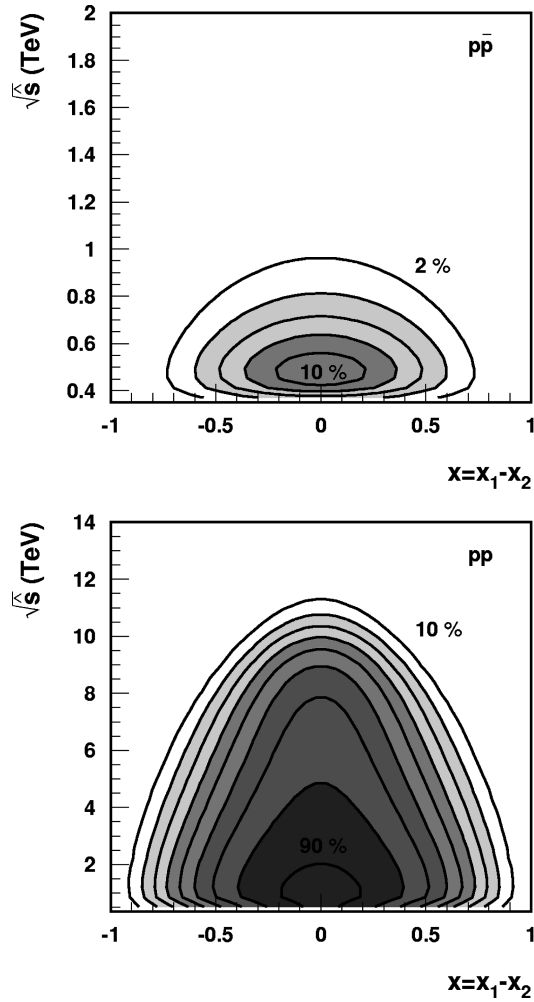


FIG. 11. Relative amount of gluon-gluon-initiated processes as a function of $x_1 - x_2 = 2P_3(t\bar{t}g)/\sqrt{s}$ and \hat{s} in lowest order, for $\sqrt{s} = 2$ TeV in proton-antiproton collisions and $\sqrt{s} = 14$ TeV in proton-proton collisions. Contour lines go from 2% (white) to 10% (dark) in steps of 2% in the former case and from 10% (white) to 90% (dark) in steps of 10% in the later (CTEQ-1).

negative x is dominated by initial \bar{q} with small x_1 and q with large x_2 . The charge asymmetry implies that $Q(\bar{Q})$ is preferentially emitted into the direction of $q(\bar{q})$, Figs. 13a,13b. The same line of reasoning is applicable for positive x , with $Q(\bar{Q})$ again preferentially emitted in the direction of $q(\bar{q})$, and the role of x_1 and x_2 reversed. In total this leads to a slight preference for centrally produced antiquarks and quarks slightly dominant in the forward and backward directions, i.e., at large positive and negative rapidities.

The differential charge asymmetry

$$A_{pp}(y) = \frac{\frac{dN(Q)}{dy} - \frac{dN(\bar{Q})}{dy}}{\frac{dN(Q)}{dy} + \frac{dN(\bar{Q})}{dy}} \quad (18)$$

is shown in Fig. 14a for top quark production at the LHC ($\sqrt{s} = 14$ TeV). As expected, a sizable charge asymmetry is

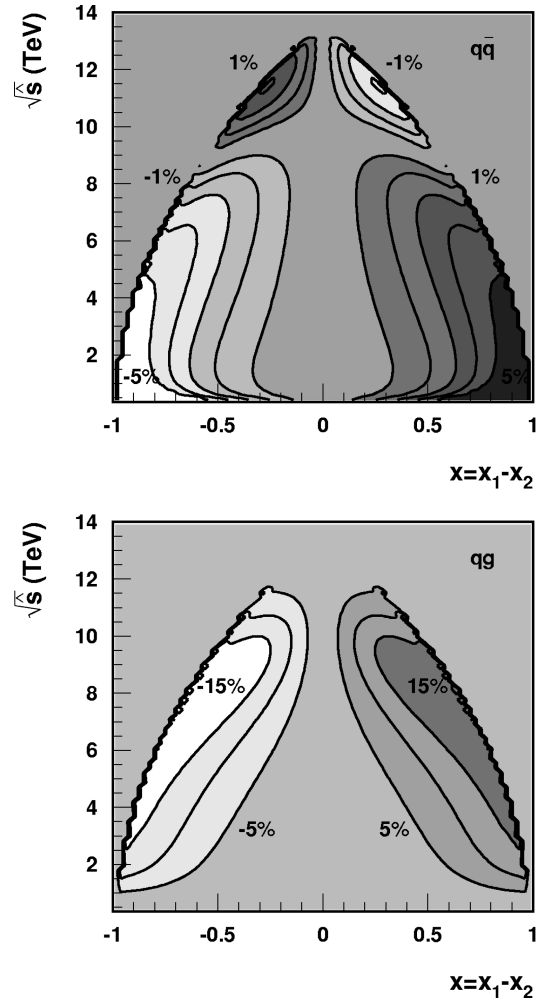


FIG. 12. Contributions from $q\bar{q}$ and $qg(\bar{q}g)$ induced reactions to the charge asymmetry in proton-proton collisions, $\sqrt{s} = 14$ TeV, as a function of $x_1 - x_2 = 2P_3(t\bar{t}g)/\sqrt{s}$ and \hat{s} . Partonic rest frame (CTEQ-1).

predicted in the region of large rapidity. It remains to be seen if the low event rates in these extreme regions will permit observation of this effect. The quark-gluon process is again negligible.

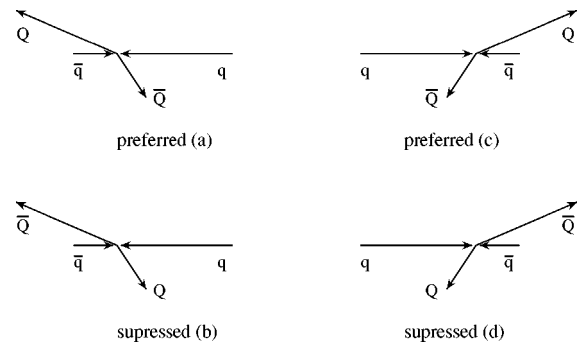


FIG. 13. Typical configuration of momenta for top quark and top antiquark production through quark annihilation in the region of large parallel momenta.

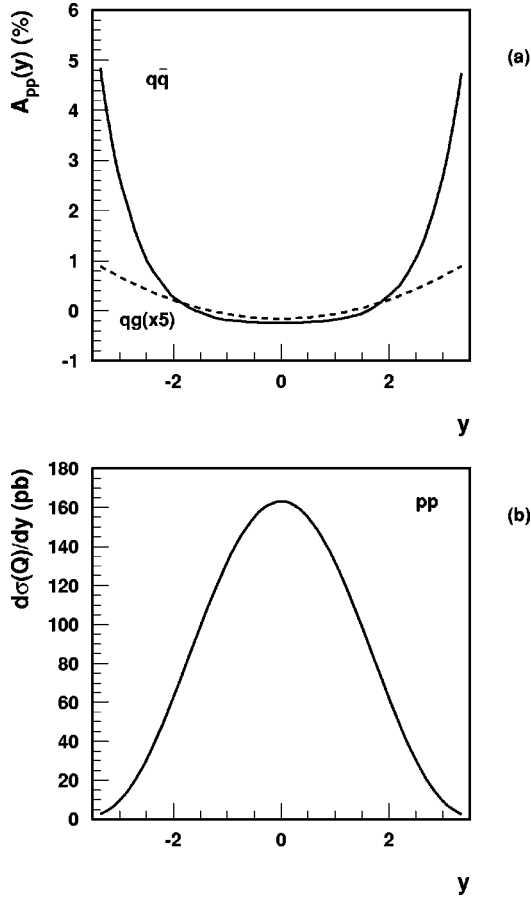


FIG. 14. Rapidity distribution of charge asymmetry (a) and total cross section at Born order (b) of top quark production in proton-proton collisions, $\sqrt{s}=14$ TeV and $\mu=m_t$. Contributions from $q\bar{q}$ fusion and flavor excitation, qg ($\bar{q}g$), are shown separately. Laboratory frame (CTEQ-1).

IV. CONCLUSIONS

The difference between the distributions of quarks versus antiquarks produced in hadronic collisions has been investigated. This asymmetry is particularly relevant for the production of top quarks in suitably chosen kinematical regions, but can also be observed for bottom quarks at large \hat{s} . At the partonic level it amounts up to 10% or even 15%. In proton-antiproton collisions at the Tevatron the integrated forward-backward asymmetry amounts close to 5%. At the LHC a slight preference for centrally produced top antiquarks is predicted, with top quarks more abundant at large positive and negative rapidities.

ACKNOWLEDGMENTS

We would like to acknowledge useful discussions with R.K. Ellis, T. Sjöstrand, and M. Seymour. This work was supported by BMBF under Contract No. 057KA92P and DFG under Contract No. Ku 502/8-1. G.R. acknowledges financial support from INFN and the TTP Institute at the University of Karlsruhe for the kind hospitality during the completion of this work.

APPENDIX: BASIC FORMULAS

For completeness we summarize here the charge-antisymmetric contributions to the heavy quark production cross section. The charge-asymmetric piece of the hard gluon radiation process

$$q(p_1) + \bar{q}(p_2) \rightarrow Q(p_3) + \bar{Q}(p_4) + g(p_5), \quad (\text{A1})$$

defined as

$$d\sigma_A^{q\bar{q}} \equiv \frac{1}{2} [d\sigma(q\bar{q} \rightarrow QX) - d\sigma(q\bar{q} \rightarrow \bar{Q}X)], \quad (\text{A2})$$

is given by

$$\begin{aligned} \frac{d\sigma_A^{q\bar{q}, \text{hard}}}{dy_{35} dy_{45} d\Omega} &= \frac{\alpha_s^3}{4\pi\hat{s}} \frac{d_{abc}^2}{16N_C^2} \frac{1}{y_{12}(y_{34} + 2m^2)y_{35}} \\ &\times \left\{ \frac{y_{13}}{y_{15}} (y_{13}^2 + y_{14}^2 + y_{23}^2 + y_{24}^2 \right. \\ &\quad \left. + 2m^2(y_{34} + 2m^2 + y_{12})) + 4m^2 y_{24} \right\} \\ &\quad - (1 \leftrightarrow 2) - (3 \leftrightarrow 4) + (1 \leftrightarrow 2, 3 \leftrightarrow 4), \end{aligned} \quad (\text{A3})$$

with $N_C=3$ and $d_{abc}^2=40/3$. All the quantities are normalized to the partonic center-of-mass energy \hat{s} ,

$$y_{ij} = 2(p_i \cdot p_j)/\hat{s}, \quad m^2 = m_Q^2/\hat{s}. \quad (\text{A4})$$

The asymmetry is explicitly driven by the antisymmetric exchange of momenta ($p_i \leftrightarrow p_j$).

On the other hand, soft radiation from Eq. (A1) integrated in phase space up to a cut in the soft gluon energy, E_{cut}^g , plus the virtual corrections to the Born process $q\bar{q} \rightarrow Q\bar{Q}$ contribute to the asymmetry as

$$\begin{aligned} \frac{d\sigma_A^{q\bar{q}, \text{virt} + \text{soft}}}{d \cos \hat{\theta}} &= \frac{\alpha_s^3}{2\hat{s}} \frac{d_{abc}^2}{16N_C^2} \beta \left\{ B(c) - B(-c) + (1 + c^2 + 4m^2) \right. \\ &\quad \left. \times \left[4 \log \left(\frac{1-c}{1+c} \right) \log(2w) + D(c) - D(-c) \right] \right\}, \end{aligned} \quad (\text{A5})$$

with

$$\beta = \sqrt{1 - 4m^2}, \quad c = \beta \cos \hat{\theta}, \quad w = E_{cut}^g/\sqrt{\hat{s}}, \quad (\text{A6})$$

and the functions $B(c)$, coming from the box contribution, and $D(c)$, from soft radiation, defined as

$$\begin{aligned}
B(c) &= \frac{1-c^2-8m^2}{1-c-2m^2} \log\left(\frac{1-c}{2}\right) \\
&+ (c+2m^2) \left[2\text{Li}_2\left(1-\frac{2m^2}{1-c}\right) - \log^2\left(\frac{1-c}{2}\right) \right] \\
&+ \frac{4c}{\beta^2} \frac{2-c^2-7m^2}{(1-2m^2)^2-c^2} m^2 \log(m^2) + \frac{c}{2} \log^2(m^2) \\
&- \frac{c}{2\beta^3} (1-8m^2+8m^4) \left[\log^2\left(\frac{1-\beta}{1+\beta}\right) \right. \\
&\left. + 4\text{Li}_2\left(-\frac{1-\beta}{1+\beta}\right) + \frac{\pi^2}{3} \right] - c \frac{\pi^2}{6}, \quad (\text{A7})
\end{aligned}$$

$$\begin{aligned}
D(c) &= 2 \text{Re} \left\{ \text{Li}_2\left(\frac{-x}{1-y}\right) - \text{Li}_2\left(\frac{1-x}{1-y}\right) \right. \\
&\left. - \text{Li}_2\left(\frac{1+x}{y}\right) + \text{Li}_2\left(\frac{x}{y}\right) \right\} + \log^2\left|\frac{y}{1-y}\right| - \text{Re Li}_2(x^2) \\
&+ \frac{1}{2} \log^2(x^2) - \log(x^2) \log(1-x^2), \quad (\text{A8})
\end{aligned}$$

where

$$x = \frac{1-c}{\sqrt{2(1-c-2m^2)}}, \quad y = \frac{1}{2} [1-\beta + \sqrt{2(1-c-2m^2)}]. \quad (\text{A9})$$

In the limit $m \rightarrow 0$ these functions simplify considerably:

$$\begin{aligned}
B(c) &= \left[1+c-c \log\left(\frac{1-c}{2}\right) \right] \log\left(\frac{1-c}{2}\right), \\
D(c) &= \log^2\left(\frac{1-c}{2}\right) - 2\text{Li}_2\left(\frac{1-c}{2}\right), \quad (\text{A10})
\end{aligned}$$

and become also free of final-state collinear divergences since only integrable divergences appear at $c=1$.

The charge-asymmetric contribution of the flavor excitation process

$$q(p_1) + g(p_2) \rightarrow Q(p_3) + \bar{Q}(p_4) + q(p_5), \quad (\text{A11})$$

defined as

$$d\sigma_A^{qg} \equiv \frac{1}{2} [d\sigma(qg \rightarrow QX) - d\sigma(qg \rightarrow \bar{Q}X)], \quad (\text{A12})$$

is given by

$$\begin{aligned}
\frac{d\sigma_A^{qg}}{dy_{35} dy_{45} d\Omega} &= \frac{\alpha_s^3}{4\pi\hat{s}} \frac{d_{abc}^2}{16N_C^2} \frac{1}{y_{15}(y_{34}+2m^2)y_{23}} \\
&\times \left\{ \left(\frac{y_{13}}{y_{12}} - \frac{y_{35}}{y_{25}} \right) [y_{13}^2 + y_{14}^2 + y_{35}^2 + y_{45}^2 \right. \\
&+ 2m^2(y_{34}+2m^2-y_{15})] \\
&\left. + 4m^2(y_{45}+y_{14}) \right\} - (3 \leftrightarrow 4). \quad (\text{A13})
\end{aligned}$$

It is infrared finite and can be obtained just by crossing of momenta from Eq. (A3).

For the convenience of the reader we also list the Born cross section for $q\bar{q}$ and gg fusion:

$$\frac{d\sigma^{q\bar{q} \rightarrow Q\bar{Q}}}{d \cos \hat{\theta}} = \alpha_s^2 \frac{T_F C_F}{N_C} \frac{\pi \beta}{2\hat{s}} (1+c^2+4m^2), \quad (\text{A14})$$

$$\begin{aligned}
\frac{d\sigma^{gg \rightarrow Q\bar{Q}}}{d \cos \hat{\theta}} &= \alpha_s^2 \frac{\pi \beta}{2\hat{s}} \left(\frac{1}{N_C(1-c^2)} - \frac{T_F}{2C_F} \right) \\
&\times \left(1+c^2+8m^2 - \frac{32m^4}{1-c^2} \right), \quad (\text{A15})
\end{aligned}$$

where $T_F=1/2$ and $C_F=4/3$.

-
- [1] S. Catani, ‘‘QCD at high-energies,’’ hep-ph/9712442, and references therein.
- [2] P. Tipton, in *Proceedings of the ICHEP 96*, Warsaw, Poland, edited by Z. Ajduk and A. K. Wroblewski (World Scientific, Singapore, 1996), p. 123.
- [3] G. Marchesini *et al.*, *Comput. Phys. Commun.* **67**, 465 (1992).
- [4] T. Sj strand, *Comput. Phys. Commun.* **82**, 74 (1994).
- [5] R. K. Ellis, in *Strong Interactions and Gauge Theories*, edited by J. Tran Thanh Van (Editions Fronti re, Gif-sur-Yvette, 1986), p. 339.
- [6] P. Nason, S. Dawson, and R. K. Ellis, *Nucl. Phys.* **B327**, 49 (1989).
- [7] W. Beenakker, W. L. van Neerven, R. Meng, G. A. Schuler, and J. Smith, *Nucl. Phys.* **B351**, 507 (1991).
- [8] F. Halzen, P. Hoyer, and C. S. Kim, *Phys. Lett. B* **195**, 74 (1987).
- [9] F. A. Berends, K. J. F. Gaemers, and R. Gastmans, *Nucl. Phys.* **B63**, 381 (1973).
- [10] F. A. Berends, R. Kleiss, S. Jadach, and Z. Was, *Acta Phys. Pol. B* **14**, 413 (1983).
- [11] A. D. Martin, R. G. Roberts, and W. J. Stirling, *Phys. Lett. B* **387**, 419 (1996).
- [12] H. L. Lai, *Phys. Rev. D* **55**, 1280 (1997).
- [13] J. H. K hn and G. Rodrigo, *Phys. Rev. Lett.* **81**, 49 (1998).
- [14] R. Bonciani, S. Catani, M. L. Mangano, and P. Nason, *Nucl. Phys.* **B529**, 424 (1998).